ACS NANO

www.acsnano.org

ARTICLE

Antimicrobial PEGtides: A Modular Poly(ethylene glycol)-Based Peptidomimetic Approach to Combat Bacteria

Minseong Kim,[#] Wonsik Mun,[#] Woo Hyuk Jung,[#] Joonhee Lee, Gayoung Cho, Jisoo Kwon, Dong June Ahn,* Robert J. Mitchell,* and Byeong-Su Kim*

Cite This: *ACS Nano* 2021, 15, 9143−9153

Read Online

ACCESS | Metrics & More | Article Recommendations | Supporting Information

ABSTRACT: **Despite their high potency, the widespread implementation of natural antimicrobial peptides is still challenging due to their low scalability and high hemolytic activities. Herein, we address these issues by employing a modular approach to mimic the key amino acid residues present in antimicrobial peptides, such as lysine, leucine, and serine, but on the highly biocompatible poly(ethylene glycol) (PEG) backbone. A series of these PEG-based peptides (PEGtides) were developed using functional epoxide monomers, corresponding to each key amino acid, with several possessing highly potent bactericidal activities and controlled selectivities, with respect to their hemolytic behavior. The critical role of the composition and the structure of the PEGtides in their selectivities was further supported by coarse-grained molecular dynamic simulations. This modular approach is anticipated to provide the design principles necessary for the future development of antimicrobial polymers.**

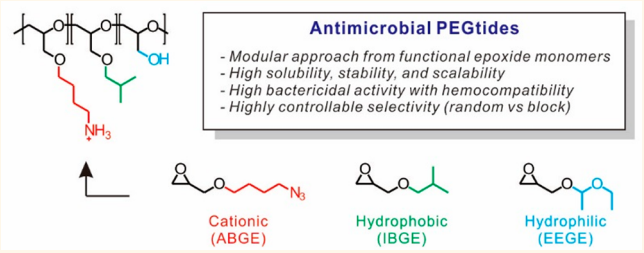

KEYWORDS: *polymeric antimicrobials, polyethers, functional epoxide monomer, peptidomimetics, molecular dynamic simulation*

INTRODUCTION

The increasing threat of multi-drug-resistant bacteria is a public health concern worldwide.[1] Thus, there is a long-standing interest in the development of antibiotics. Antimicrobial peptides (AMPs), a natural part of the autoimmune system of most organisms, have been recognized as a promising solution to address the emergence of this global challenge.[2] AMPs are amphiphilic oligopeptides generally composed of 30−50 amino acids,[2−4] majorly cationic amino acids, which promote their interaction with the negatively charged bacterial membrane.[5] Subsequently, the hydrophobic amino acids present in the AMPs allow them to slide into the phospholipid bilayer and destabilize the membrane.[2,5] In addition, the rigid polypeptide backbone of the AMP provides a regular arrangement of functional groups, increasing its bactericidal effect. Despite their potent antimicrobial activities, widespread use of natural AMPs is still challenging due to low scalability, which contributes to their high cost of production,[2,6] their inactivation by proteases,[7,8] and their high hemolytic activities.[9]

To address these issues, various synthetic antimicrobial polymers possessing diverse functional moieties have been suggested,[10−22] including polymers constructed with different backbones, such as polyoxazoline, polyacrylate, poly(2-hydroxyethyl methacrylate), and polyacrylamide.[14,23−26] However, polymers with an all-carbon backbone are structurally rigid but suffer from poor aqueous solubilities. Alternatively, an antimicrobial polymer platform that has not been explored in the literature is PEG, which can offer several benefits, including flexibility, solubility, high biocompatibility, and nonimmunogenicity.[27,28]

Therefore, we suggest here a peptidomimetic approach that combines the advantages of a PEG backbone with the amino acid residues commonly found in natural AMPs, *i.e.*, lysine, leucine, and serine, leading to PEG-based peptides (PEGtides). It is of note that the term "PEGtide" is more relevant to functionalized linear polyglycerols; however, to highlight the structural features of the polyether backbone developed in this study, we have opted to use this term.[29] Specifically, we

Received: March 29, 2021
Accepted: May 10, 2021
Published: May 14, 2021

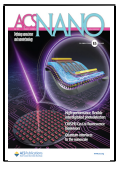

https://doi.org/10.1021/acsnano.1c02644
ACS Nano 2021, 15, 9143−9153

Scheme 1. Design and synthesis of antimicrobial PEGtides. (Left) Structure of antimicrobial peptides (AMPs) and their key constitutional amino acid composition and (right) antimicrobial PEG-based peptides (PEGtides) with corresponding functional epoxide monomers.

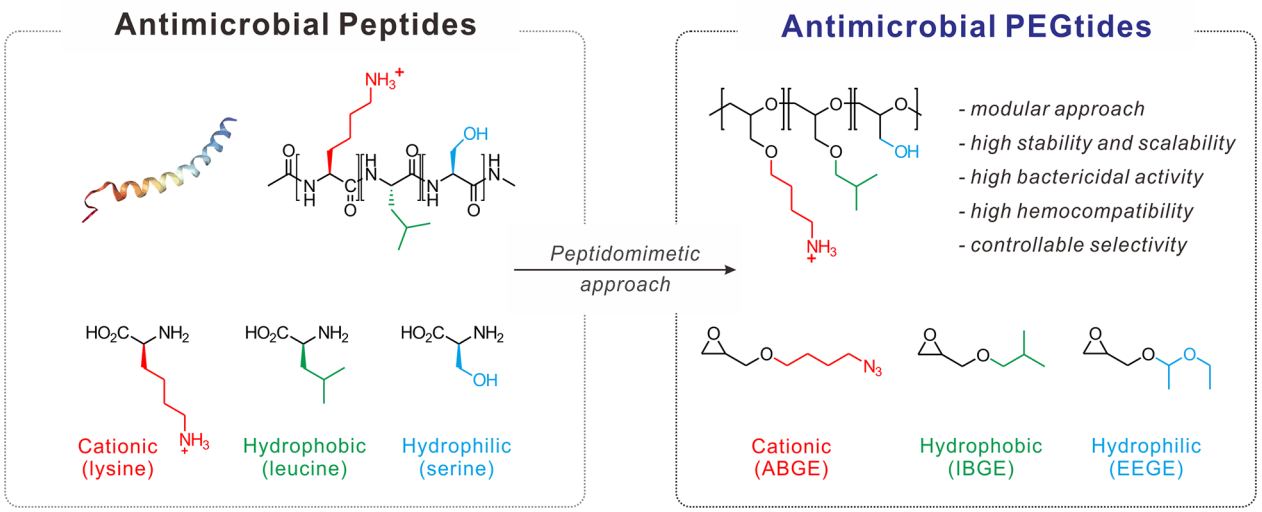

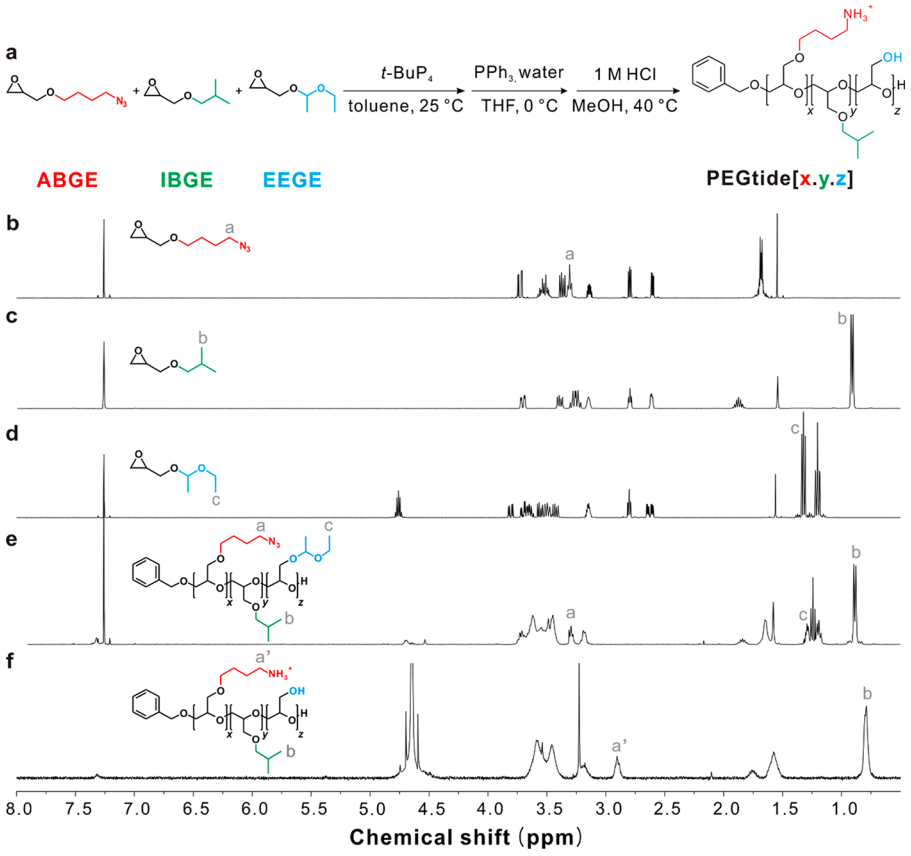

Figure 1. Design and synthesis of antimicrobial PEGtides. (a) Synthetic scheme of antimicrobial PEGtides. (b–f) Representative ^{1}H NMR spectra of the (b) ABGE monomer, (c) IBGE monomer, (d) EEGE monomer, (e) P(ABGE$_{10}$-*co*-IBGE$_{10}$-*co*-EEGE$_{10}$) copolymer (*i.e.*, pre-PEGtide), and (f) PEGtide[10.10.10]. All samples were measured in $CDCl_3$ except (f) in D_2O.

successfully developed a library of well-defined, functional epoxide monomers that mimic these three amino acid residues, *i.e.*, azidobutyl glycidyl ether (ABGE), isobutyl glycidyl ether (IBGE), and ethoxyethyl glycidyl ether (EEGE), which were used to synthesize the pre-PEGtide polymers *via* anionic ring-opening polymerization (Scheme 1). Subsequent deprotection and reduction of the polymers yielded a series of functional PEGtides with controlled side chain functionalities arranged on a highly flexible polyether backbone.

An additional benefit of this platform was the fine control it provided over the functional monomers used to construct the PEGtide, permitting the synthesis of homo, random, and block copolymers for each through stoichiometry and the sequence of monomer addition. Within this study, therefore, the

https://doi.org/10.1021/acsnano.1c02644
ACS Nano 2021, 15, 9143–9153

Table 1. Characterization of PEGtides Prepared in This Study[a]

PEGtides[x.y.z][b]	composition (NMR)	NMR M_n (g/mol)[c]	GPC M_n (g/mol)[c]	$Đ$[d]	NMR M_n (g/mol)[e]	zeta potential mV
[30.0.0][f]	$PABGE_{30}$	5240	5600	1.22	4420	+46.4
[0.30.0]	$PIBGE_{25}$	3370	3230	1.07	3370	
[0.0.30]	$PEEGE_{26}$	3900	3010	1.07	2030	
[25.5.0]	$P(ABGE_{24}$-*co*-$IBGE_3)$	4500	4830	1.11	3850	+29.3
[20.10.0]	$P(ABGE_{20}$-*co*-$IBGE_{10})$	4830	4560	1.17	4310	+40.2
[15.15.0]	$P(ABGE_{14}$-*co*-$IBGE_{14})$	4330	5480	1.11	3970	+57.3
[15.0.15]	$P(ABGE_{13}$-*co*-$EEGE_{14})$	4300	4300	1.07	2970	+45.8
[10.20.0]	$P(ABGE_9$-*co*-$IBGE_{20})$	4140	4260	1.25	3910	+38.0
[10.10.10]	$P(ABGE_{10}$-*co*-$IBGE_{10}$-*co*-$EEGE_{11})$	4640	4770	1.08	3560	+47.1
[5.25.0]	$P(ABGE_4$-*co*-$IBGE_{22})$	4490	4390	1.06	3440	+5.92
[0.15.15]	$P(IBGE_{12}$-*co*-$EEGE_{12})$	3270	3230	1.06	2420	
[25-5-0][g]	$P(ABGE_{25}$-*b*-$IBGE_6)$	5170	4750	1.23	4520	+54.2
[20-10-0]	$P(ABGE_{20}$-*b*-$IBGE_{10})$	4830	4480	1.20	4310	+45.7

[a]The number indicates the respective monomers as PEGtide [ABGE.IBGE.EEGE]. [b]PEGtide[cationic.hydrophobic.hydrophilic]. [c]Protected P(ABGE-*co*-IBGE-*co*-EEGE) polymers. [d]Determined by GPC in $CHCl_3$, PMMA calibration. [e]Deprotected PEGtides. [f]Random copolymers. [g]Block copolymers.

activities of different PEGtides against several different pathogenic bacterial strains were evaluated. In parallel, their hemolytic activities were also determined to select those that have the greatest selectivity. The critical role of the microstructure of PEGtides (random *vs* block) in the selectivity was further analyzed using coarse-grained molecular dynamic (CG-MD) simulations to understand the preferential interactions occurring between these PEGtides and the bacterial membranes/lipids.

RESULTS AND DISCUSSION

Polymer Design and Synthesis. A well-defined, functional epoxide monomer library, mimicking key amino acid residues, *i.e.*, lysine, leucine, and serine, commonly found in natural AMPs was constructed. This glycidyl ether-based ternary monomer system included three compounds—ABGE, IBGE, and EEGE (Figure 1a)—which were selected on the basis of previous studies.[30,31] All monomers were synthesized by a simple substitution reaction (typical isolated yields of 41–76%) and purified by a fractional distillation to high purity (>99%; Figure 1a–d and Figures S1–S7 in the Supporting Information).

Copolymerization proceeded *via* organic superbase *t*-BuP_4-catalyzed anionic ring-opening polymerization of the monomers using benzyl alcohol as an initiator in toluene at room temperature (Figure 1e). The highly basic *t*-BuP_4 was chosen, as it allowed controlled polymerization of the respective monomers at room temperature. A series of copolymers with tunable ratios between each functional moiety (*i.e.*, cationic, hydrophobic, and hydrophilic) were achieved by controlling the monomer feed ratio and the sequence of the monomer addition during the preparation of each PEGtide, while random copolymerization was carried out by increasing the proportion of the hydrophobic segment (*i.e.*, IBGE) in the reaction from 11% to 86%. It is important to note that the degree of polymerization in each case was fixed as 30, which was selected since it is similar to the number of amino acids present in many natural AMPs.[3,32] The prepared copolymers were thoroughly characterized by ^1H and ^{13}C NMR and GPC (Figures S8–S12).

As shown in Figure 1e, the ^1H NMR spectra for the P(ABGE-*co*-IBGE-*co*-EEGE) copolymer clearly possesses the characteristic peaks found in the respective monomers incorporated within (Figure 1b–d). Furthermore, the GPC results of the copolymers exhibited a monomodal distribution and narrow dispersity ($Đ$ = 1.06–1.25) (Table 1 and Figures S13, S14). When polymerization was carried out by mixing monomers, an experiment was conducted to measure the reactivity ratio to confirm whether random copolymers were formed as expected. The reactivity ratio between the pair of monomers was examined using *in situ* ^{13}C NMR spectroscopy with inverse-gated decoupling. The plot of total conversion against monomer conversion was presented to determine reactivity ratios for the pair of monomers, resulting in r_{ABGE} = 0.649 ± 0.01 and r_{IBGE} = 1.586 ± 0.07 (Figure S15). These results suggest the random statistical copolymerization of ABGE and IBGE without any gradient in the microstructure of the polymers. Subsequently, these copolymers were treated with PPh_3 and H_2O in THF, followed by 1.0 M HCl, to yield the desired PEGtide with its free amines and hydroxyl groups after Staudinger reduction and hydrolysis of the respective monomers, as revealed in the ^1H NMR spectra (Figure 1f). In parallel, other PEGtides were likewise synthesized, including block copolymers PEGtide[25-5-0] and PEGtide[20-10-0], and characterized by ^1H NMR and GPC (Figure S16–S21).

Successful liberation of the free amine groups in the PEGtides was confirmed by their highly positive zeta-potential values (Table 1). This is an important feature of the PEGtides, and AMPs in general, as these cationic groups increase interactions with negatively charged lipids present in bacterial cellular membranes, which impacts their bactericidal activities (Figure 2a). In contrast, the hydroxyl moiety (from EEGE) itself does not impart a noticeable antimicrobial activity (Figure 2a and Table S1), and, thus, focus was given to evaluating random copolymers composed of the cationic and hydrophobic blocks, *i.e.*, ABGE and IBGE, respectively.

Antibacterial Assays. The bactericidal effects of each PEGtide were then evaluated based on the ratio of the monomers and their microstructure using three Gram-negative strains (*E. coli*, *A. baumannii*, and *P. aeruginosa*) and two Gram-positive strains (*S. aureus* and *E. faecium*). Many of the PEGtides were highly bactericidal, with minimum inhibitory concentrations (MICs) that were micromolar (Figure 2a and Table S1). For example, one of the more active constructs

https://doi.org/10.1021/acsnano.1c02644
ACS Nano 2021, 15, 9143–9153

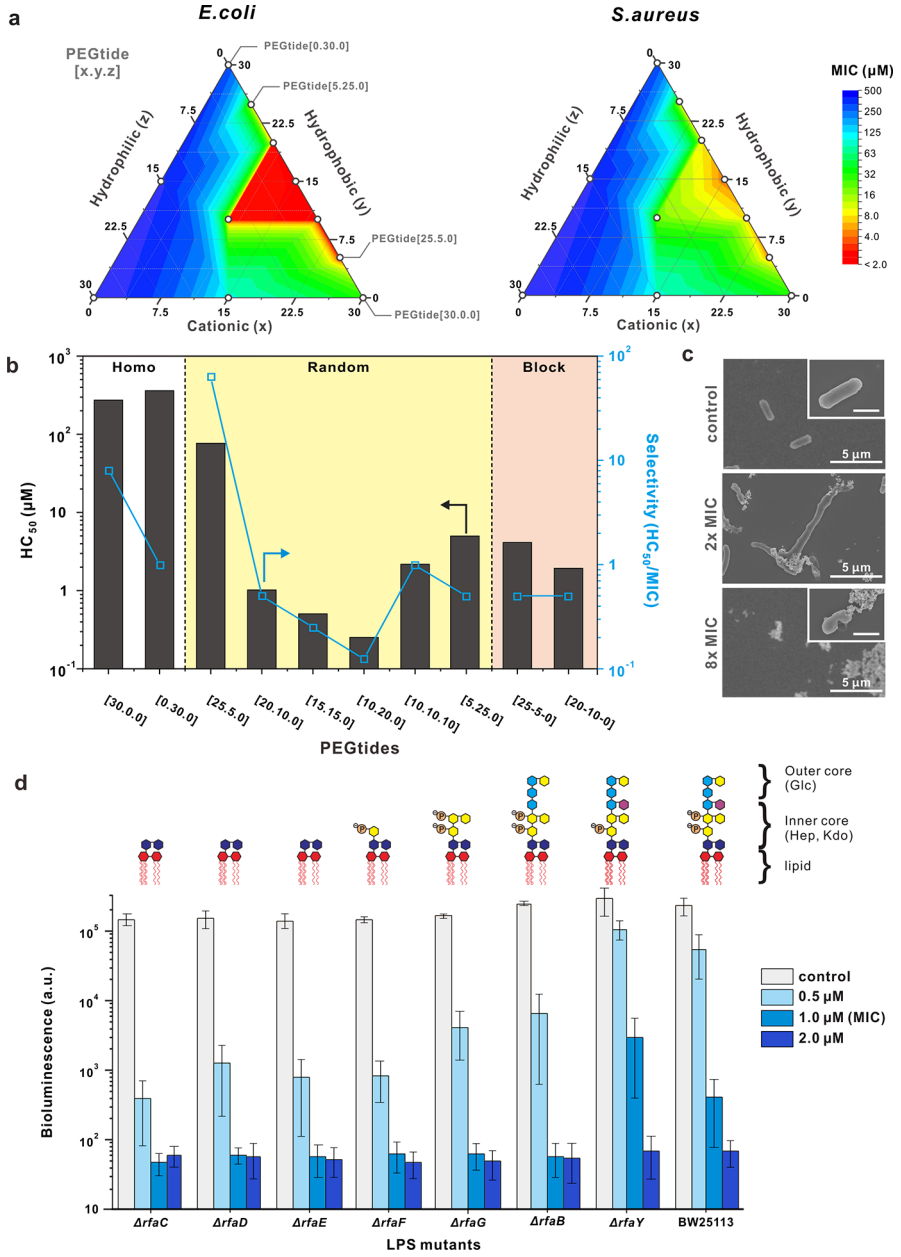

Figure 2. Antimicrobial and hemocompatibility assays of PEGtides. (a) Ternary contour maps of minimum inhibitory concentration (MIC) of all PEGtides synthesized toward (left) Gram-negative *E. coli* MG1655 and (right) Gram-positive *S. aureus* ATCC 25923. Note that the open circle in the map indicates the respective PEGtides tested. Each vertex of the ternary contour map represents a homopolymer. (b) Hemocompatibility and selectivity assays with various PEGtides in homo, random, and block structures. Representative selectivity was determined using the MIC values of *E. coli* (n = 3). (c) Representative SEM images of *E. coli* after treatment with PEGtide[25.5.0] in varying concentration. Inset scale bar is 1 μm. (d) Antimicrobial activity of PEGtide[25.5.0] toward several LPS mutants with *E. coli* BW25113/pDRec3 measured based upon the loss in bioluminescence at 2 h. Each test was performed independently in triplicate, and the standard deviations for each are plotted as the error bars.

(PEGtide[25.5.0]) had an MIC toward *E. coli* of 1.01 μM, a concentration that is comparable to that of other highly active antimicrobial polymers.[18] Interestingly, no bactericidal effects were observed for two of the homopolymers, *i.e.*, PEGtide[0.30.0] and PEGtide[0.0.30], both of which lack any cationic moieties, reinforcing the idea that the cationic moiety plays a critical role in the bactericidal efficacy of AMPs. We thus focused on modulating the relative ratio between the cationic and hydrophobic moieties.

Although many of the PEGtide formulations were active against the different pathogenic strains tested (Table S1), for their potential downstream application, such as in wound dressings or as oral antibiotics, several other factors need be evaluated, including their hemocompatibility and stability. In general, as shown in Figure 2b, the hemolytic activity of the PEGtides (calculated as the concentration leading to 50% lysis of the red blood cells (RBCs), *i.e.*, HC_{50}) increased as the hydrophobic fraction in the copolymer increased, implying these side chains enhance interactions between the PEGtide and the membranes of the RBCs. This translated into lower selectivities for these PEGtides, defined as the ratios between HC_{50} and MIC (HC_{50}/MIC), a result that is similar to that of

https://doi.org/10.1021/acsnano.1c02644
ACS Nano 2021, 15, 9143−9153

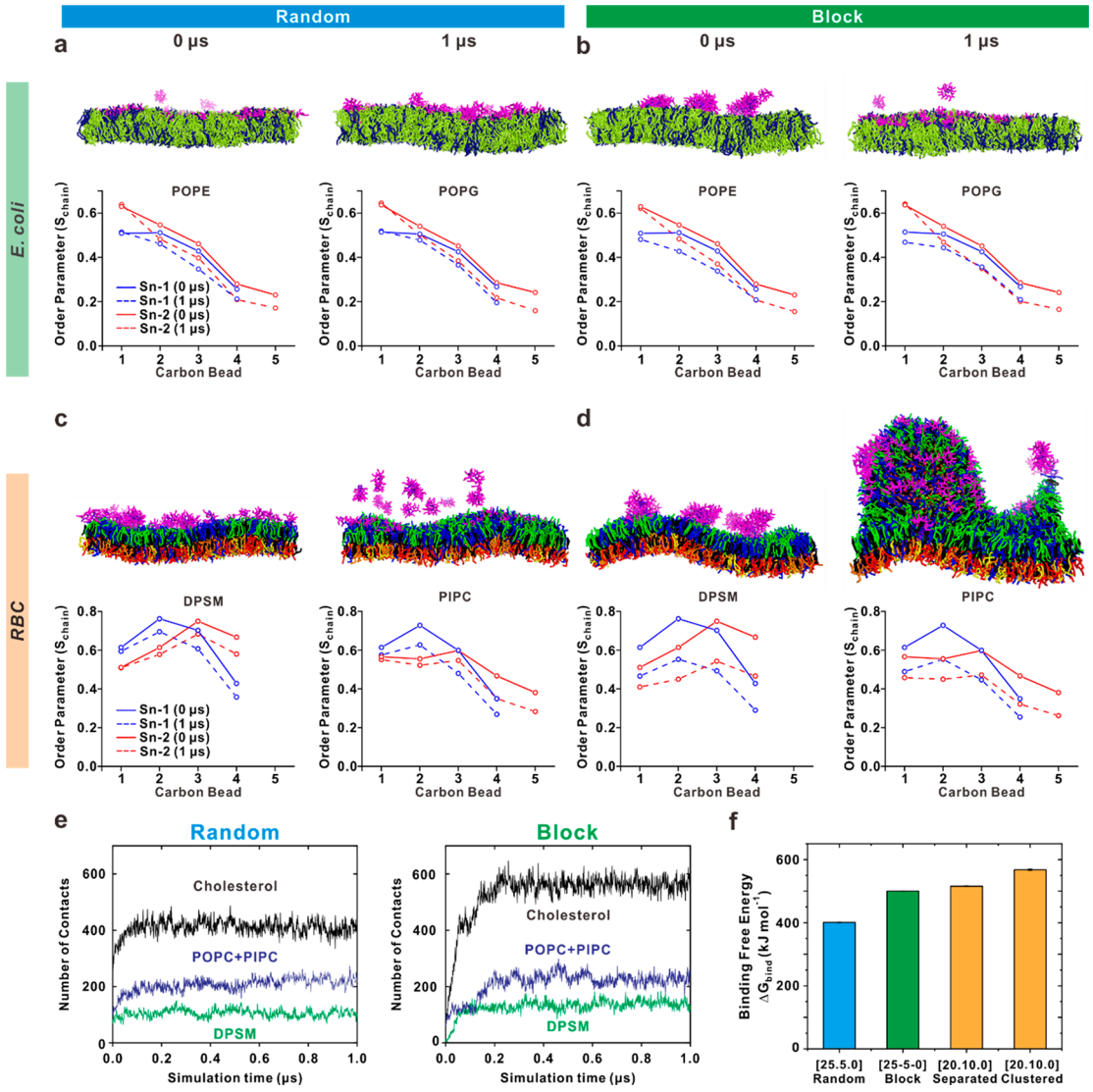

Figure 3. CG-MD simulations for comparing the effects of random and block PEGtides on *E. coli* and RBC membranes. (a–d) Representative time-lapse snapshots of membrane simulations with corresponding analysis of order parameters with membrane lipids. (a) Random PEGtide[25.5.0] on an *E. coli* membrane with POPE:POPG lipids; (b) block PEGtide[25-5-0] on an *E. coli* membrane with POPE:POPG lipids. Note that the overall number of copolymers is fixed to 30, and three block copolymers comprise one copolymer aggregate. (c) Random PEGtide[25.5.0] on an RBC membrane with DPSM:POPC lipids; (d) block PEGtide[25-5-0] on an RBC membrane with DPSM:POPC lipids. (e) Number of contacts between hydrophobic moiety of (left) random PEGtide[25.5.0] and (right) block PEGtide[25-5-0] with (black) cholesterol, (blue) POPC and PIPC, and (green) DPSM. (f) Calculated binding free energy of (blue) random PEGtide[25.5.0], (green) block PEGtide[25-5-0], and (orange) separated and clustered PEGtide[20.10.0] with an RBC membrane from umbrella sampling simulations. Note that parameters presented in (a)–(d) are as follows: (blue) Sn-1 and (red) Sn-2 lipid acyl chain order parameters of lipids at the (solid line) initial and (dotted line) final time point of simulation. See other simulation details in the Supporting Information.

other studies.[3,17,18] With a value of 64, however, PEGtide[25.5.0] was the most selective antimicrobial copolymer of those tested and is even significantly better than MSI-78, a derivative of magainin, which has a moderate selectivity of 9.6.[33] The next best copolymer (with a selectivity value of 8) was PEGtide[30.0.0], but, as listed in Table S1, its MICs were significantly higher, leading to its rejection. Likewise, many of the other PEGtides had selectivity values less than 1, indicating that, although they may be highly active against bacterial pathogens, such as PEGtide[15.15.0] (Table S1), they were more active toward the RBCs. Consequently, only PEGtide[25.5.0] was selected for further characterization.

The second criterion is stability. While PEGtide[25.5.0] was stable during its preparation, where high temperature (70 °C, 6 h) and acidic conditions (1 M HCl) were used, one of the main advantages of synthetic antimicrobial polymers over conventional proteinaceous AMPs is their superior stability against proteolysis. This was also true of PEGtide[25.5.0], as treatment with either trypsin or proteinase K for 30 min did not diminish its antibacterial activities, showing this copolymer is both stable and robust (Figure S22).

Subsequent experiments of PEGtide[25.5.0] with *E. coli* were performed to understand the underlying antimicrobial mechanisms. As shown in Figure 2c, *E. coli* cells exposed to either 2 or 8 μM PEGtide[25.5.0] displayed structural defects,

https://doi.org/10.1021/acsnano.1c02644
ACS Nano 2021, 15, 9143–9153

i.e., filamentous cells and membrane rupturing, suggesting this copolymer was attacking the cellular membranes. This was validated using an assay to quantify the amount of cellular ATP that leaked after treatment, as in a previous study.[34] Marked increases in the extracellular ATP concentrations were observed when the bacteria were treated with 0.5 μM (0.5× MIC) PEGtide[25.5.0] (Figure S23), while this plateaued at above 95% when 1× MIC or higher concentrations were used. These results clearly prove PEGtide[25.5.0] attacks the cellular membrane, causing significant perturbations that lead to a leakage of the cytoplasmic contents.

Expanding on this idea, the first structure PEGtide[25.5.0] would encounter when interacting with Gram-negative bacterial strains is their lipopolysaccharide (LPS), the dominant glycolipid in the external leaflet of the outer membrane, where it functions both in membrane stabilization and as a barrier against antibiotics.[35] Since adaptive changes in bacterial physiology are a conserved theme in infections, including the modulation of LPS synthesis and structure to aid pathogens in evading the immune response, establishing a persistent inflammation, and in developing increased resistance to antimicrobials,[36] we evaluated the potential role the LPS plays in *E. coli*'s responses to PEGtide[25.5.0]. Figure S24 shows a strong correlation between the bioluminescence from the *E. coli* strain[37] and its surviving population, implying the bioluminescence can be used as a proxy to evaluate viability. Subsequently, the efficacy of PEGtide[25.5.0] was evaluated against a number of *E. coli* strains that produce LPS of varying lengths (Figure 2d).[38,39] When compared against the wild-type cells, those strains producing the shortest LPS, *i.e.*, the Δ*rfaC*, Δ*rfaD*, Δ*rfaE*, Δ*rfaF*, and Δ*rfaG* mutants, were all more susceptible to PEGtide[25.5.0]. These results show that PEGtide[25.5.0] remained as effective against these mutants as the wild-type strain. Moreover, the bioluminescence data in Figure 2d was from a two-hour exposure. Based on the correlation shown in Figure S24, this would mean that the vast majority of the *E. coli* present were killed by 1 μM PEGtide[25.5.0] within this period, suggesting rapid killing kinetics. This was evaluated further where the optical density of the *E. coli* cultures was monitored (Figure S25). Clear differences were seen in less than 30 min, confirming PEGtide[25.5.0] rapidly attacks the membranes of this microbe, leading to a rupturing of cells, as shown in Figure 2c, and a concomitant loss in optical density.

Coarse-Grained Molecular Dynamic Simulations. It was reported previously that the block copolymers possessed a higher selectivity than random copolymers, owing to charge segregation.[18,40] In contrast to those reports, the block PEGtide[25-5-0] developed here was markedly more hemolytic (*i.e.*, 16-fold lower HC_{50}) than the random PEGtide[25.5.0] (Figure 2a). We postulated that this difference is mainly related to (1) the relative spacing between hydrophobic units and (2) the hydrophilic and flexible polymer backbone of the PEGtides, which may facilitate interactions between the polymers and the cellular membranes. Accordingly, the concentrated presence of cationic and hydrophobic portions within defined regions of the block polymers may help them associate in complexes that interact more easily through multivalent interactions with the RBC membrane, leading to its eventual disruption. In the random polymers, this would be mitigated by the assorted placement of the monomers, which would act to minimize their activities toward RBC membranes while maintaining their attraction toward, and action against, those present in bacteria. We explored this further theoretically *via* CG-MD simulations, specifically assessing the self-assembly behaviors of random and block PEGtides toward the constituent lipids present in *E. coli* and RBC membranes.

Based on the initial optimization simulations, the block PEGtide[25-5-0] formed larger clusters composed of three copolymers within the initial 2 μs, whereas random PEGtide[25.5.0] remained as a single polymer chain (Figure S26 and Table S2). Consequently, all the following simulations were conducted using these two configurations, with them positioned close to either the *E. coli* or RBC membranes. For the simulations with *E. coli* membranes, the constituent lipids were palmitoyloleoylphosphatidylethanolamine (POPE) and palmitoyloleoylphosphatidylglycerol (POPG). In both cases, adsorption of the copolymers to the membrane surface occurred within the first 200 ns, where they remained in a surface-bound state until the end of the simulations (Figure 3a,b and Figures S27, S28).

The effects these surface-bound PEGtides had on the *E. coli* membranes were quantified using the lipid bilayer structural characteristics, including the area per lipid (Figure S29) and the order parameters along the Sn-1 and Sn-2 acyl chains of the lipid molecules (Figure 3a,b and Figure S30). Top views of the POPE:POPG membrane interacting with the random PEGtide and two-dimensional plots represented the area per lipid for each POPE and POPG (Figure S31). An increase in area per lipid was highly pronounced in the vicinity of surface-bound polymers. Upon adsorption, the area per lipid molecule around random PEGtides increased from 0.62 nm^2 to 0.75 nm^2. Additionally, adsorption of the random PEGtides decreased the POPE and POPG lipid acyl chain order parameters, leading to a more disordered membrane state, which is consistent with the experimental results. Similar results were obtained when the block PEGtides were used in the simulations, implying the different microstructures present in these two PEGtides do not have a significant impact on their activity toward the POPE:POPG membrane found in *E. coli*.

We then switched the simulations to RBC membranes to explore the observed differences in the random and block PEGtides hemolytic activities (Figure 3c,d). Similar to the simulations performed above, the equilibrated configurations of both PEGtides were placed in close proximity to the RBC membrane with its constituent lipids, including sphingomyelin lipid with *N*-stearoyl-D-erythro tails (DPSM), phosphatidylcholine lipid with 1-palmitoyl-2-linoleoyl tails (PIPC), phosphatidylcholine lipid with 1-palmitoyl-2-oleoyl tails (POPC), and a large number of cholesterol molecules. The snapshots of the initial and final configurations of both simulations demonstrate that there are considerable differences between the random and block PEGtides. Focusing on the random PEGtide[25.5.0], 17 of the 30 polymers used in the simulation bound the RBC membrane surface within 200 ns, while 13 polymers remained as assembled structures in aqueous solution until the end of the simulation (Figure S32). In contrast, 27 of block PEGtide[25-5-0] polymers bound the RBC membrane surface within 500 ns and, most notably, induced significant disruption of membrane bilayer structure with the formation of lipid protrusions. The size of the lipid protrusions increased within the first 1 μs and reached a plateau thereafter (Figures S33 and S34).

To distinguish between the effects of random and block PEGtides on RBCs more quantitatively, the average order parameters of the lipid molecules in the upper leaflet of the

https://doi.org/10.1021/acsnano.1c02644
ACS Nano 2021, 15, 9143−9153

RBC membrane were calculated for each (Figure 3c,d). The results indicate the order parameters for both Sn-1 and Sn-2 acyl chains are significantly lower for the RBC membrane lipid molecules after adsorption of the block PEGtides compared to those after adsorption of the random copolymers. The average order parameter for the tails of DPSM, the main component within the upper leaflet of the RBC membrane, was reduced by 0.189 when exposed to the block PEGtides, whereas it was reduced by only 0.079 with the random PEGtides. Taken together, these simulation results strongly affirm the experimental results, namely, that the random PEGtide[25.5.0] has a considerably higher selectivity for Gram-negative bacterial membranes than those of RBCs when compared to its block PEGtide counterpart.

To understand the mechanism of block PEGtide-induced membrane disruption *via* lipid protrusion more in detail, we investigated further interactions between the hydrophobic IBGE segments of random or block PEGtides, known as a key functionality inducing membrane disruption, and the membrane components, particularly the cholesterol present in the upper leaflet of the RBC membrane (Figure 3e). The results revealed the hydrophobic IBGE monomer present in both the random and block PEGtides preferentially interacts with the cholesterol, the number of interactions increasing noticeably in the case of block PEGtides: from 77 to 646 contacts within the first 300 ns of simulation. The differences between the random and block polymer activities can be explained in part by their interactions with cholesterol in the mammalian cell phospholipid bilayer. While the presence of cholesterol within the membrane makes the membrane slightly neutral, which reduces the number of interactions it has with the positively charged antimicrobial polymers or peptides, once the polymers enter the membrane, their interactions with cholesterol reportedly increase resistance toward antimicrobial polymers or peptides, as cholesterol would act to stabilize the phospholipid bilayer.[1] However, the simulations show the number of interactions between cholesterol and the block polymer are much higher than those with the random polymer. This may actually represent a case where the number of interactions is overly excessive, as the cholesterol would be sequestered and have reduced membrane-stabilizing activities, leading to the formation of membrane protrusions as observed in Figure 3d.

These results are further supported by free energy variations during the adsorption of a single block or random copolymer on the RBC membrane. As shown in Figure 3f, the binding free energy in the surface-bound state of the block PEGtide[25-5-0] showed a greater increase (approximately 100 kJ mol^{-1}) than that of the random PEGtide[25.5.0], indicating stronger interactions exist between block PEGtide[25-5-0] and the RBC membrane. When considered alongside the cholesterol results above, this result indicates stronger interactions exist between the hydrophobic monomers present in the block copolymer and the RBC membrane, leading to membrane disruption *via* lipid protrusion, which is consistent with higher hemolytic activities of block PEGtides.

These simulation results led us to hypothesize that if the number of hydrophobic monomers is identical, as their number in the local vicinity of the membrane increases, the number of interactions with cholesterols should also increase. To verify this postulation, we chose random PEGtide[20.10.0], as its selectivity (0.5) was markedly lower compared to that of random PEGtide[25.5.0] (64), whereas the bactericidal activities were similar for both PEGtides (Table S1). To quantitatively analyze the simulation results, we calculated the binding energy between the RBC membrane and each of the PEGtides. In the simulation with the random PEGtide[20.10.0] (Figure S35), the distance between the hydrophobic IBGE monomers was adjusted so that either (1) all IBGE monomers were separated by at least one monomer spacing (*i.e.*, separated) or (2) four IBGE monomers were clustered while the remaining monomers were randomly arranged (*i.e.*, clustered). As shown in Figure 3f, the binding free energy of PEGtide[20.10.0] is higher than that of both random PEGtide[25.5.0] and block PEGtide[25-5-0]. Most interestingly, the binding energy of PEGtide$[20.10.0]_{clustered}$ is higher than that of PEGtide$[20.10.0]_{separated}$, suggesting a critical role of the hydrophobic monomers in modulating the multivalent interactions with cholesterols and, thereby, the selectivity of the PEGtides.

CONCLUSION

In summary, we present here PEGtides, copolymers composed of three functional epoxide monomers (cationic, hydrophobic, and hydrophilic) that mimic the key amino acid residues found in natural antimicrobial peptides. Several of the PEGtides displayed highly potent bactericidal effects against different bacterial strains, including several pathogens. Based on its MIC values and hemolytic activities, PEGtide[25.5.0] was clearly the best, with good selectivity. Finally, the critical role of the PEGtide microstructure in governing its interactions with RBC membranes was revealed by coarse-grained molecular dynamic simulations, explaining the very different results obtained with the random PEGtide[25.5.0] and its block counterpart, PEGtide[25-5-0]. We anticipate that the modular approach described here will provide design principles to develop more effective antimicrobial polymers to combat bacterial pathogens and infections.

EXPERIMENTAL METHODS

Reagents and Methods. All solvents and reagents were purchased from commercial sources (Sigma-Aldrich, TCI, and Alfa Aesar). Toluene (99.9%) was distilled under nitrogen and stored with a molecular sieve (4 Å). ^{1}H and ^{13}C NMR spectra were recorded using an Agilent 400 MHz spectrometer equipped with an autosampler at ambient probe temperature in $CDCl_3$. All spectra were recorded in ppm units with tetramethylsilane (TMS), except the samples with D_2O. Gel permeation chromatography (GPC) measurements (Agilent 1200 series) were performed with chloroform as an eluent at 35 °C with a flow rate of 1.0 mL min^{-1} using a refractive index (RI) detector. Standard poly(methyl methacrylate) (PMMA) samples were used for calibration to determine number- and weight-averaged molecular weights (M_n and M_w). ζ-Potential was measured using a Zetasizer (Malvern Instruments Ltd.) with aqueous PEGtide solutions (1 mg mL^{-1}).

Synthesis of Azidobutyl Glycidyl Ether.[31] First, azidobutanol was prepared by mixing vacuum-distilled 4-chlorobutanol (10.7 g, 98.55 mmol) with a solution of sodium azide (9.61 g, 147.83 mmol) in 20 mL of water, and the solution was refluxed for 24 h. The crude product was dissolved in 200 mL of ethyl acetate and rinsed with water (30 mL) three times and brine (90 mL) one time. The organic layer was dried with Na_2SO_4 and evaporated using a rotary evaporator to obtain a pale yellow liquid (8.2 g, yield 70%).

Epichlorohydrin (5.78 g, 94.40 mmol) was slowly added to an aqueous solution of 50% NaOH (13.2 mL, 10.0 g, 250 mmol) at 0 °C. After stirring 15 min, azidobutanol (1.80 g, 15.63 mmol) was added dropwise over 10 min, and the solution was stirred at room temperature for 4 h. The crude product was dissolved in 200 mL of

https://doi.org/10.1021/acsnano.1c02644
ACS Nano 2021, 15, 9143−9153

ethyl acetate and rinsed with water (30 mL) three times and brine (90 mL) one time. The organic layer was dried with Na_2SO_4 and evaporated using a rotary evaporator, and the mixture was purified using silica gel column chromatography with an ethyl acetate/hexane (1:10 v/v) eluent to obtain the ABGE monomer. The ABGE monomer was further purified by vacuum distillation to obtain pure ABGE monomer as a transparent liquid (1.1 g, yield 41%) and stored with activated molecular sieves (10 wt %). ^{1}H NMR (400 MHz, $CDCl_3$): δ 3.73 (dd, J = 11.5, 2.9 Hz, 1H), 3.60−3.44 (m, 2H), 3.37 (dd, J = 11.5, 5.9 Hz, 1H), 3.31 (t, J = 6.3 Hz, 2H), 3.17−3.11 (m, 1H), 2.80 (t, J = 4.6 Hz, 1H), 2.60 (dd, J = 5.0, 2.7 Hz, 1H), 1.78−1.60 (m, 3H).

Synthesis of Isobutyl Glycidyl Ether. Epichlorohydrin (5.78 g, 94.40 mmol) was slowly added to an aqueous solution of 50% NaOH (13.2 mL, 10.0 g, 250 mmol) at 0 °C. After stirring 15 min, isobutanol (1.15 g, 15.63 mmol) was added dropwise over 10 min, and the solution was stirred at room temperature for 4 h. The crude product was dissolved in 200 mL of ethyl acetate and rinsed with water (30 mL) three times and brine (90 mL) one time. The organic layer was dried with Na_2SO_4 and evaporated using a rotary evaporator, and the mixture was purified using silica gel column chromatography with an ethyl acetate/hexane (1:10 v/v) eluent to obtain the IBGE monomer. The IBGE monomer was further purified by vacuum distillation to obtain pure IBGE monomer as a transparent liquid (1.3 g, yield 66.7%) and stored with activated molecular sieves (10 wt %). ^{1}H NMR (400 MHz, $CDCl_3$): δ 4.80−4.72 (m, 1H), 3.81 (dd, J = 11.5, 3.3 Hz, 1H), 3.70 (dd, J = 11.5, 3.3 Hz, 1H), 3.67−3.62 (m, 1H), 3.56 (dd, J = 11.6, 5.5 Hz, 1H), 3.50 (ddd, J = 9.4, 7.1, 1.1 Hz, 1H), 3.43 (dd, J = 11.5, 6.0 Hz, 1H), 3.19−3.11 (m, 1H), 2.82−2.77 (m, 1H), 2.63 (ddd, J = 14.6, 5.1, 2.7 Hz, 1H), 1.32 (dd, J = 6.2, 5.4 Hz, 1H), 1.20 (td, J = 7.1, 1.2 Hz, 1H).

Synthesis of Ethoxyethyl Glycidyl Ether. EEGE was prepared as described by Taton *et al.*[30]

Representative Synthetic Procedure of P(ABGE-*co*-IBGE-*co*-EEGE). All glassware was washed and flame-dried prior to use. A 0.125 mL solution of t-BuP_4 (0.80 M, 0.10 mmol) in n-hexane was added to a 1.2 mL solution of benzyl alcohol (10.67 μL, 0.1 mmol) in toluene under a N_2 atmosphere. A premixed solution of ABGE (170 mg, 1 mmol), IBGE (130 mg, 1 mmol), and EEGE (146 mg, 1 mmol) was added to the solution. The reaction was monitored by ^{1}H NMR to determine residual epoxide signals. When polymerization was determined to be complete, the reaction mixture was quenched with an excess amount of benzoic acid. The mixture was passed through a basic alumina pad using THF to remove residual t-BuP_4. The polymer solution was concentrated *in vacuo* to obtain P(ABGE-*co*-IBGE-*co*-EEGE) (450 mg, yield 88%); this was confirmed by ^{1}H NMR and GPC. ^{1}H NMR (400 MHz, $CDCl_3$): δ 7.37−7.30 (m, 5H), 4.72−4.67 (m, 11H), 4.54 (s, 2H), 3.78−3.40 (m, 216H), 3.33−3.26 (m, 19H), 3.19 (s, 20H), 1.91−1.77 (m, 10H), 1.65 (d, J = 2.7 Hz, 39H), 1.30 (t, J = 6.9 Hz, 32H), 1.22−1.15 (m, 33H), 0.89 (d, J = 6.6 Hz, 61H). $M_{n,NMR}$ = 4640 g mol^{-1}. GPC ($CHCl_3$, PMMA standard) $M_{n,GPC}$ = 4770 g mol^{-1} and $Đ$ = 1.08.

General Synthesis Procedure of Block P(ABGE-*b*-IBGE). All glassware was washed and flame-dried before polymerization. A 0.125 mL solution of t-BuP_4 (0.80 M, 0.10 mmol) in n-hexane was added to a 1.2 mL solution of benzyl alcohol (10.67 μL, 0.10 mmol) in toluene under a N_2 atmosphere. Then, ABGE (342 mg, 2.0 mmol) was added to this solution. The reaction was monitored using ^{1}H NMR spectroscopy to determine residual epoxide signals. After reaction completion, a small aliquot of the crude P(ABGE) polymer was taken for GPC analysis. Additional IBGE (130 mg, 1 mmol) was added to the solution, and the reaction was monitored by ^{1}H NMR to determine the residual epoxide signals. When the reaction was determined to be complete, an excess amount of benzoic acid was added to terminate polymerization. The mixture was passed through a basic alumina pad using THF to remove residual t-BuP_4. The polymer solution was concentrated *in vacuo* to obtain P(ABGE-*b*-IBGE) (420 mg); this was confirmed by ^{1}H NMR and GPC. ^{1}H NMR (400 MHz, $CDCl_3$): δ 6.98 (s, 5H), 4.54 (s, 2H), 3.53 (m, 204H), 3.29 (d, J = 6.5 Hz, 40H), 3.23−3.13 (m, 20H), 1.91−1.78 (m, 10H), 1.65 (d, J = 3.3 Hz, 83H), 0.89 (d, J = 6.7 Hz, 64H). $M_{n,NMR}$ = 4830 g mol^{-1} and DP_{NMR}: ABGE/IBGE = 20/10. GPC ($CHCl_3$, PMMA standard) $M_{n,GPC}$ = 4480 g mol^{-1} and $Đ$ = 1.20.

Synthesis of the PEGtides. A typical procedure for the Staudinger reduction and hydrolysis of ABGE- and EEGE-containing polymers is as follows: P(ABGE-*co*-IBGE-*co*-EEGE) (100 mg, 0.22 mmol of azide) was dissolved in 1.0 mL of THF in an ice bath, and the solution was degassed *via* N_2 bubbling for 20 min. When PPh_3 (144 mg, 0.55 mmol) was completely dissolved in the solution, water (0.01 mL, 0.55 mmol) was added to the mixture and stirred for 12 h at room temperature. THF was removed under reduced pressure, and a solution of 1.0 M HCl in MeOH (1:1, v/v) was added to acidify and dissolve the polymer. The acidic aqueous phase was stirred at 60 °C for 2 h. The reaction mixture was washed three times with diethyl ether to remove residual triphenylphosphine and triphenylphosphine oxide. The resulting aqueous solution was condensed and dried under high vacuum to give 72 mg of a pale yellow powder of PEGtides[10.10.10] as shown in Table 1. ^{1}H NMR (400 MHz, D_2O): δ 7.33 (m, 5H), 4.48 (m, 2H) 3.52 (m, 217H), 3.17 (m, 20H), 2.90 (m, 21H), 1.74 (m, 11H), 1.57 (m, 41H), 0.79 (m, 31H).

Copolymerization Kinetics. A mixture of benzyl alcohol (1.0 equiv) and ABGE and IBGE (15 equiv each) in toluene-d_8 (2.5 M to the total amount of monomers) was transferred by a syringe to a conventional NMR tube sealed with a rubber septum. To the NMR tube was added t-BuP_4 (1.0 equiv), and it was shaken to homogenize the mixture before placing it in the NMR spectrometer. The sample temperature was set to 27 °C, and the first spectrum was recorded 11 min after t-BuP_4 was added and continuously recorded every 16 min with 256 scans for 6 h by an inverse-gated ^{13}C mode. The integrals of the methine carbon of each monomer (δ = 28.44 ppm for IBGE and 77.85 ppm for ABGE) were monitored to calculate monomer conversion in reference to the residual signal of toluene (20.40 ppm).

Bactericidal Assays. To determine the minimum inhibitory concentration for each of the PEGtides, we employed Clinical & Laboratory Standards Institute (CLSI) protocols as described previously.[41] Briefly, the different bacterial strains used (*Escherichia coli* MG1655, *Pseudomonas aeruginosa* PAO1, *Staphylococcus aureus* ATCC 25923, and clinical isolates of *Enterococcus faecium* and *Acinetobacter baumannii*) were grown on Mueller−Hinton agar plates overnight at 37 °C, and a single colony was used to inoculate 5 mL of Mueller−Hinton broth (MHB). After overnight incubation with shaking at 37 °C and 250 rpm, the bacterial culture was diluted 100-fold into fresh MHB and grown for 1 h to allow the culture to enter the exponential phase. At this time, the cells were diluted into MHB once more to obtain a cell density of 2×10^4 to 2×10^5 colony forming units (CFU) mL^{-1}. The PEGtides were dissolved in fresh MHB media and serially diluted in a sterile, covered 96-well plate (SPL, Korea), with a final volume of 100 μL in each well. To the test wells was added an equal volume of the bacterial cultures (1:1 v/v). The plate was then covered with a lid and incubated without shaking at 37 °C for 18 h in a humidified incubator to prevent evaporation of the media. After overnight growth, the optical density (OD) of each well was measured using a plate reader (TECAN, USA) set to measure the absorbance at a wavelength of 600 nm (n = 3). The MIC was defined as the minimum concentration of PEGtides where the OD did not deviate significantly from that of the negative control (the wells containing media but without addition of bacteria). This protocol was used for each of the five bacterial strains and was repeated at least six times independently.

Bactericidal Mechanism Study. To demonstrate antimicrobial PEGtides disrupt the cellular membrane, ATP concentrations within the supernatant were determined. Cultures of *E. coli* MG1655 were grown as above to the midexponential phase in MHB media and exposed to several different concentrations of the random PEGtide[25.5.0] (0, 0.5× MIC, 1× MIC, and 4× MIC). After incubating at 37 °C without shaking for 2 h, the culture was split, and ATP concentration within the whole culture (supernatant and cells) was determined. For this, ATP was extracted using a 2.5% trichloroacetic acid solution for 1 h using the Enliten ATP assay kit (Promega, Madison, WI), as described previously.[42] Simultaneously,

https://doi.org/10.1021/acsnano.1c02644
ACS Nano 2021, 15, 9143−9153

the cells were removed by filtration through a 0.22 μm PES membrane (Millex, Millipore), and the ATP concentration in the supernatant was also determined using the same kit.

To determine if treating the bacteria caused any cellular morphology changes, scanning electron microscopy (SEM) was used. First, *E. coli* MG1655 cultures were grown in MHB for 1 h as described above until the culture entered the exponential phase, and they were exposed to the random PEGtide[25.5.0] at several different concentrations (0, 2× MIC, and 8× MIC). After incubating for 2 h at 37 °C without shaking, the cells were fixed using a 2.5% glutaraldehyde solution and prepared for SEM.

Hemolytic Activity of the PEGtides. The hemolytic activities of the AMPs were tested using fresh sheep RBCs as described previously.[25] Briefly, the RBCs were diluted 20-fold (v/v) in phosphate-buffered saline (PBS, pH 7.4), pelleted, and washed three times using PBS before resuspending in the original volume (at 5%). Equal volumes of the RBCs and PEGtide solution (150 μL each) were mixed in a sterile tube. For the negative and positive controls, PBS buffer alone and 1% Triton X-100 in PBS were used, respectively. The different samples were incubated under shaking at 37 °C and 150 rpm for 2 h. After centrifugation to pellet the cells (8000*g*, 10 min), 100 μL aliquots of the supernatant were transferred to the wells of a clear 96-well plate (SPL, Korea), and the absorbance (A) at 485 nm was measured using a TECAN plate reader (n = 3). The percent hemolysis was calculated using the following equation: Hemolysis (%) = $(A_{\text{PEGtide}} - A_{\text{negative}})/(A_{\text{positive}} - A_{\text{negative}}) \times 100$. The selectivity of the PEGtides was then calculated using the ratio of the concentration leading to 50% hemolysis (HC_{50}) against the MIC for the microbes.[33,43]

Coarse-Grained Molecular Dynamics Simulation of Self-Assembly of PEGtides. To simulate the self-assembly process for both random and block PEGtides, two models for antimicrobial PEGtides were represented by 89 coarse-grained (CG) beads. The differences in chemical structures between random PEGtides and block PEGtides were captured by CG models with different distributions of cationic beads and hydrophobic beads. For the random PEGtides model, the positions of hydrophobic beads were randomly selected. For the block PEGtides model, the positions of hydrophobic beads were selected based on experimental results. Bead types and nonbonded interactions of side chains of PEGtides that mimic amino acids were parametrized based on a previously reported force field by Marrink et al.[44] The backbone of the polymers was parametrized based on the Martini force field using the results from all-atom simulations (Figure S36). The bead types of the backbone of the polymers were determined by calculating the partitioning free energies of the building blocks from water to octanol. The Bennett acceptance ratio method was used to calculate the free energy of system in water and in octanol. The bonded parameters for the CG model were fitted based on the results from all-atom models (Tables S3 and S4). The self-assembly simulation of random and block PEGtides began with 30 copolymers randomly distributed in 130 000 CG water beads, representing 520 000 water molecules. Periodic boundary conditions were applied in the x, y, and z directions with an initial cell size of 25 × 25 × 25 nm^3. After 100 ns equilibrium steps, the self-assembly simulations were performed for 2 μs at 298 K.

CG-MD Simulation for PEGtides on the Lipid Membrane. To elucidate the effects of random and block copolymers on the lipid membrane, four separate systems were built, using either random or block PEGtides on a POPE:POPG membrane representing the bacterial membrane of *E. coli* and an RBC membrane model reported previously.[45] Both lipid bilayers were generated with the CHARMM-GUI membrane builder.[46] All lipid membrane systems were solvated with at least 25 water beads per lipid and ionized with 150 mM of both Na^+ and Cl^- ions. Starting structures of both random and block PEGtides were generated from the self-assembly simulation. Four main starting models were built using random and block PEGtides: 30 random PEGtides were inserted close to both the POPE:POPG membrane and RBC membrane; 10 assembled structures of three block PEGtides were inserted close to both the POPE:POPG membrane and RBC membranes. After 100 ns equilibration steps, production runs were conducted for 1 and 2.5 μs for the POPE:POPG systems and RBC systems, respectively.

To calculate the binding energy of the random and block PEGtides with the POPE:POPG membrane and RBC membrane, the potential of mean force (PMF) for the adsorption of random and block copolymer on the membrane was calculated by umbrella sampling. For the simulation, we built a membrane system (10 × 10 × 10 nm^3) with one polymer. Initially, a single random PEGtide or a block PEGtide was inserted close to the membrane systems, *i.e.*, either the POPE:POPG membrane or the RBC membrane. The four systems were initially equilibrated for 500 ns to obtain initial configurations for umbrella sampling. To generate the z directional reaction coordinate, the pull code with pulling distance calculated relative to the center of the membrane was used. For the POPE:POPG systems with random and block PEGtides, 34 windows with a spacing of 0.1 nm each were created to cover the range from 2.2 to 5.5 nm using a force constant of 1000 kJ mol^{-1} nm^{-2}. For the RBC systems with random and block copolymers, 39 windows with a spacing of 0.1 nm each were created to cover the range from 2.2 to 6.0 nm using a force constant of 1000 kJ mol^{-1} nm^{-2}. Each window was equilibrated for 50 ns prior to carrying out 100 ns production runs. PMF was measured using the WHAM tools in the GROMACS package. The binding energy was calculated based on the differences between the highest and lowest energy state forms within the PMF curve.

System Parameters for CG-MD Simulation. The simulation of PEGtides was conducted with Gromacs 5.1.4[47] using the MARTINI force field.[48] A V-rescale thermostat[49] was used to control the temperature. The pressure of the system was maintained at 1 bar using the Berendsen[50] and Parrinello−Raman barostats[51] for the equilibrium and production run, respectively. All simulations were conducted using a leapfrog integrator with a time-step of 20 fs. A Verlet cutoff scheme with a buffer tolerance of 0.005 kJ mol^{-1} was used, and neighbor lists were updated every 20 steps. Coulomb interactions were calculated by the reaction-field method with a cutoff range of 1.1 nm and a dielectric constant of 15. van der Waals interactions were also calculated using the cutoff range of 1.1 nm. The linear constraint solver (LINCS) algorithm was used to constrain the bond lengths.[52]

Analysis Details for CG-MD Simulation. To quantify the interaction between the hydrophobic moiety and lipid molecules, the numbers of contacts was calculated. We define the hydrophobic monomer contacting lipids as those lipid molecules that have at least one CG bead within 0.6 nm from hydrophobic monomers of random or block copolymers. The same procedure was used to define lipids interacting with copolymers. For the analysis of membrane order, the lipid order parameter is calculated according to $S = \left\{\frac{3\cos^2\theta - 1}{2}\right\}$. θ is the angle between the vectors of two consecutive beads and the z axis.

ASSOCIATED CONTENT

Supporting Information

The Supporting Information is available free of charge at https://pubs.acs.org/doi/10.1021/acsnano.1c02644.

Synthetic protocols, detailed ^{1}H and ^{13}C NMR spectra of the monomer; ^{1}H NMR spectra, GPC, data and polymerization kinetics of PEGtides; detailed MIC profiles of PEGtides, bactericidal kinetics, and ATP leakage test; CG-MD simulation model, self-assembly simulation of PEGtides, time-lapse snapshots of membrane simulation, and additional MD simulation data (PDF)

AUTHOR INFORMATION

Corresponding Authors

Dong June Ahn − *Department of Chemical and Biological Engineering and KU-KIST Graduate School of Converging Science and Technology, Korea University, Seoul 02841,*

https://doi.org/10.1021/acsnano.1c02644
ACS Nano 2021, 15, 9143−9153

Republic of Korea; orcid.org/0000-0001-5205-9168; Email: ahn@korea.ac.kr

Robert J. Mitchell − *School of Life Sciences, Ulsan National Institute of Science and Technology (UNIST), Ulsan 44919, Republic of Korea;* orcid.org/0000-0002-9608-5381; Email: esgott@unist.ac.kr

Byeong-Su Kim − *Department of Chemistry, Yonsei University, Seoul 03722, Republic of Korea;* orcid.org/0000-0002-6419-3054; Email: bskim19@yonsei.ac.kr

Authors

Minseong Kim − *Department of Chemistry, Yonsei University, Seoul 03722, Republic of Korea; Department of Chemistry, Ulsan National Institute of Science and Technology (UNIST), Ulsan 44919, Republic of Korea;* orcid.org/0000-0002-2612-922X

Wonsik Mun − *School of Life Sciences, Ulsan National Institute of Science and Technology (UNIST), Ulsan 44919, Republic of Korea;* orcid.org/0000-0001-5980-7210

Woo Hyuk Jung − *Department of Chemical and Biological Engineering, Korea University, Seoul 02841, Republic of Korea;* orcid.org/0000-0001-5169-4223

Joonhee Lee − *Department of Chemistry, Yonsei University, Seoul 03722, Republic of Korea; Department of Chemistry, Ulsan National Institute of Science and Technology (UNIST), Ulsan 44919, Republic of Korea*

Gayoung Cho − *School of Life Sciences, Ulsan National Institute of Science and Technology (UNIST), Ulsan 44919, Republic of Korea*

Jisoo Kwon − *School of Life Sciences, Ulsan National Institute of Science and Technology (UNIST), Ulsan 44919, Republic of Korea*

Complete contact information is available at: https://pubs.acs.org/10.1021/acsnano.1c02644

Author Contributions

[#]M.K., W.M., and W.H.J. contributed equally to this work.

Notes

The authors declare no competing financial interest.

ACKNOWLEDGMENTS

This work was primarily supported by Samsung Research Funding & Incubation Center of Samsung Electronics under Project Number SRFC-MA1602-07. This work was also supported by the National Research Foundation of Korea (NRF-2021R1A2C3004978, NRF-2020R1A2C2012158, and NRF-2021R1A2C3009955).

REFERENCES

(1) Zasloff, M. Antimicrobial Peptides of Multicellular Organisms. *Nature* **2002**, *415* (6870), 389−395.

(2) Hancock, R. E. W.; Sahl, H. G. Antimicrobial and Host-Defense Peptides as New Anti-Infective Therapeutic Strategies. *Nat. Biotechnol.* **2006**, *24* (12), 1551−1557.

(3) Ergene, C.; Yasuhara, K.; Palermo, E. F. Biomimetic Antimicrobial Polymers: Recent Advances in Molecular Design. *Polym. Chem.* **2018**, *9* (18), 2407−2427.

(4) Gagnon, M. C.; Strandberg, E.; Grau-Campistany, A.; Wadhwani, P.; Reichert, J.; Bürck, J.; Rabanal, F.; Auger, M.; Paquin, J. F.; Ulrich, A. S. Influence of the Length and Charge on the Activity of α-Helical Amphipathic Antimicrobial Peptides. *Biochemistry* **2017**, *56* (11), 1680−1695.

(5) Kuroda, K.; DeGrado, W. F. Amphiphilic Polymethacrylate Derivatives as Antimicrobial Agents. *J. Am. Chem. Soc.* **2005**, *127* (12), 4128−4129.

(6) Spohn, R.; Daruka, L.; Lázár, V.; Martins, A.; Vidovics, F.; Grézal, G.; Méhi, O.; Kintses, B.; Számel, M.; Jangir, P. K.; Csörgő, B.; Györkei, Á.; Bódi, Z.; Faragó, A.; Bodai, L.; Földesi, I.; Kata, D.; Maróti, G.; Pap, B.; Wirth, R.; et al. Integrated Evolutionary Analysis Reveals Antimicrobial Peptides with Limited Resistance. *Nat. Commun.* **2019**, *10* (1), 4538.

(7) Porter, E. A.; Weisblum, B.; Gellman, S. H. Mimicry of Host-Defense Peptides by Unnatural Oligomers: Antimicrobial β-Peptides. *J. Am. Chem. Soc.* **2002**, *124* (25), 7324−7330.

(8) Meng, H.; Kumar, K. Antimicrobial Activity and Protease Stability of Peptides Containing Fluorinated Amino Acids. *J. Am. Chem. Soc.* **2007**, *129* (50), 15615−15622.

(9) Zhao, J.; Zhao, C.; Liang, G.; Zhang, M.; Zheng, J. Engineering Antimicrobial Peptides with Improved Antimicrobial and Hemolytic Activities. *J. Chem. Inf. Model.* **2013**, *53* (12), 3280−3296.

(10) Lienkamp, K.; Madkour, A. E.; Musante, A.; Nelson, C. F.; Nüsslein, K.; Tew, G. N. Antimicrobial Polymers Prepared by ROMP with Unprecedented Selectivity: A Molecular Construction Kit Approach. *J. Am. Chem. Soc.* **2008**, *130* (30), 9836−9843.

(11) Sadrearhami, Z.; Yeow, J.; Nguyen, T. K.; Ho, K. K. K.; Kumar, N.; Boyer, C. Biofilm Dispersal Using Nitric Oxide Loaded Nanoparticles Fabricated by Photo-PISA: Influence of Morphology. *Chem. Commun.* **2017**, *53* (96), 12894−12897.

(12) Takahashi, H.; Caputo, G. A.; Vemparala, S.; Kuroda, K. Synthetic Random Copolymers as a Molecular Platform to Mimic Host-Defense Antimicrobial Peptides. *Bioconjugate Chem.* **2017**, *28* (5), 1340−1350.

(13) Huang, K. S.; Yang, C. H.; Huang, S. L.; Chen, C. Y.; Lu, Y. Y.; Lin, Y. S. Recent Advances in Antimicrobial Polymers: A Mini-Review. *Int. J. Mol. Sci.* **2016**, *17* (9), 1578.

(14) Judzewitsch, P. R.; Nguyen, T. K.; Shanmugam, S.; Wong, E. H. H.; Boyer, C. Towards Sequence-Controlled Antimicrobial Polymers: Effect of Polymer Block Order on Antimicrobial Activity. *Angew. Chem., Int. Ed.* **2018**, *57* (17), 4559−4564.

(15) Palermo, E. F.; Kuroda, K. Structural Determinants of Antimicrobial Activity in Polymers Which Mimic Host Defense Peptides. *Appl. Microbiol. Biotechnol.* **2010**, *87* (5), 1605−1615.

(16) Krumm, C.; Harmuth, S.; Hijazi, M.; Neugebauer, B.; Kampmann, A. L.; Geltenpoth, H.; Sickmann, A.; Tiller, J. C. Antimicrobial Poly(2-Methyloxazoline)s with Bioswitchable Activity through Satellite Group Modification. *Angew. Chem., Int. Ed.* **2014**, *53* (15), 3830−3834.

(17) Nguyen, T. K.; Lam, S. J.; Ho, K. K. K.; Kumar, N.; Qiao, G. G.; Egan, S.; Boyer, C.; Wong, E. H. H. Rational Design of Single-Chain Polymeric Nanoparticles That Kill Planktonic and Biofilm Bacteria. *ACS Infect. Dis.* **2017**, *3* (3), 237−248.

(18) Oda, Y.; Kanaoka, S.; Sato, T.; Aoshima, S.; Kuroda, K. Block *versus* Random Amphiphilic Copolymers as Antibacterial Agents. *Biomacromolecules* **2011**, *12* (10), 3581−3591.

(19) Namivandi-Zangeneh, R.; Kwan, R. J.; Nguyen, T. K.; Yeow, J.; Byrne, F. L.; Oehlers, S. H.; Wong, E. H. H.; Boyer, C. The Effects of Polymer Topology and Chain Length on the Antimicrobial Activity and Hemocompatibility of Amphiphilic Ternary Copolymers. *Polym. Chem.* **2018**, *9* (13), 1735−1744.

(20) Grace, J. L.; Huang, J. X.; Cheah, S. E.; Truong, N. P.; Cooper, M. A.; Li, J.; Davis, T. P.; Quinn, J. F.; Velkov, T.; Whittaker, M. R. Antibacterial Low Molecular Weight Cationic Polymers: Dissecting the Contribution of Hydrophobicity, Chain Length and Charge to Activity. *RSC Adv.* **2016**, *6* (19), 15469−15477.

(21) Chin, W.; Zhong, G.; Pu, Q.; Yang, C.; Lou, W.; De Sessions, P. F.; Periaswamy, B.; Lee, A.; Liang, Z. C.; Ding, X.; Gao, S.; Chu, C. W.; Bianco, S.; Bao, C.; Tong, Y. W.; Fan, W.; Wu, M.; Hedrick, J. L.; Yang, Y. Y. A Macromolecular Approach to Eradicate Multidrug Resistant Bacterial Infections while Mitigating Drug Resistance Onset. *Nat. Commun.* **2018**, *9* (1), 917.

(22) Sadrearhami, Z.; Nguyen, T. K.; Namivandi-Zangeneh, R.; Jung, K.; Wong, E. H. H.; Boyer, C. Recent Advances in Nitric Oxide Delivery for Antimicrobial Applications Using Polymer-Based Systems. *J. Mater. Chem. B* **2018**, *6* (19), 2945−2959.
(23) Bixler, G. D.; Bhushan, B. Review Article: Biofouling: Lessons from Nature. *Philos. Trans. R. Soc., A* **2012**, *370* (1967), 2381−2417.
(24) Kitagawa, H.; Takeda, K.; Kitagawa, R.; Izutani, N.; Miki, S.; Hirose, N.; Hayashi, M.; Imazato, S. Development of Sustained Antimicrobial-Release Systems Using Poly(2-Hydroxyethyl Methacrylate)/Trimethylolpropane Trimethacrylate Hydrogels. *Acta Biomater.* **2014**, *10* (10), 4285−4295.
(25) Judzewitsch, P. R.; Zhao, L.; Wong, E. H. H.; Boyer, C. High-Throughput Synthesis of Antimicrobial Copolymers and Rapid Evaluation of Their Bioactivity. *Macromolecules* **2019**, *52* (11), 3975−3986.
(26) Sovadinova, I.; Palermo, E. F.; Urban, M.; Mpiga, P.; Caputo, G. A.; Kuroda, K. Activity and Mechanism of Antimicrobial Peptide-Mimetic Amphiphilic Polymethacrylate Derivatives. *Polymers* **2011**, *3* (3), 1512−1532.
(27) Knop, K.; Hoogenboom, R.; Fischer, D.; Schubert, U. S. Poly(Ethylene Glycol) in Drug Delivery: Pros and Cons as Well as Potential Alternatives. *Angew. Chem., Int. Ed.* **2010**, *49* (36), 6288−6308.
(28) Fahrländer, E.; Schelhaas, S.; Jacobs, A. H.; Langer, K. PEGylated Human Serum Albumin (HSA) Nanoparticles: Preparation, Characterization and Quantification of the PEGylation Extent. *Nanotechnology* **2015**, *26* (14), 145103.
(29) Hibbitts, A.; O'Connor, A. M.; McCarthy, J.; Forde, É. B.; Hessman, G.; O'Driscoll, C. M.; Cryan, S. A.; Devocelle, M. Poly(Ethylene Glycol)-Based Peptidomimetic "PEGtide" of Oligo-Arginine Allows for Efficient SiRNA Transfection and Gene Inhibition. *ACS Omega* **2019**, *4* (6), 10078−10088.
(30) Taton, D.; Le Borgne, A.; Sepulchre, M.; Spassky, N. Synthesis of Chiral and Racemic Functional Polymers from Glycidol and Thioglycidol. *Macromol. Chem. Phys.* **1994**, *195* (1), 139−148.
(31) Lee, J.; Han, S.; Kim, M.; Kim, B. S. Anionic Polymerization of Azidoalkyl Glycidyl Ethers and Post-Polymerization Modification. *Macromolecules* **2020**, *53* (1), 355−366.
(32) Brogden, K. A. Antimicrobial Peptides: Pore Formers or Metabolic Inhibitors in Bacteria? *Nat. Rev. Microbiol.* **2005**, *3* (3), 238−250.
(33) Ilker, M. F.; Nüsslein, K.; Tew, G. N.; Coughlin, E. B. Tuning the Hemolytic and Antibacterial Activities of Amphiphilic Polynorbornene Derivatives. *J. Am. Chem. Soc.* **2004**, *126* (48), 15870−15875.
(34) Yadavalli, S. S.; Carey, J. N.; Leibman, R. S.; Chen, A. I.; Stern, A. M.; Roggiani, M.; Lippa, A. M.; Goulian, M. Antimicrobial Peptides Trigger a Division Block in *Escherichia coli* through Stimulation of a Signalling System. *Nat. Commun.* **2016**, *7*, 12340.
(35) Nikaido, H.; Vaara, M. Molecular Basis of Bacterial Outer Membrane Permeability. *Microbiol. Rev.* **1985**, *49* (1), 1−32.
(36) Maldonado, R. F.; Sá-Correia, I.; Valvano, M. A. Lipopolysaccharide Modification in Gram-Negative Bacteria during Chronic Infection. *FEMS Microbiol. Rev.* **2016**, *40* (4), 480−493.
(37) Lee, S.; Amasia, M.; Madou, M.; Mitchell, R. J. Serum Complement Enhances the Responses of Genotoxin- and Oxidative Stress-Sensitive *Escherichia coli* Bioreporters. *Biosens. Bioelectron.* **2013**, *46*, 175−182.
(38) Soh, S. M.; Lee, D. G.; Mitchell, R. J. Enhanced Microbial Fuel Cell (MFC) Power Outputs through Membrane Permeabilization Using a Branched Polyethyleneimine. *Biosens. Bioelectron.* **2020**, *170*, 112623.
(39) Soh, S. M.; Jang, H.; Mitchell, R. J. Loss of the Lipopolysaccharide (LPS) Inner Core Increases the Electrocompetence of *Escherichia coli*. *Appl. Microbiol. Biotechnol.* **2020**, *104* (17), 7427−7435.
(40) Kuroki, A.; Sangwan, P.; Qu, Y.; Peltier, R.; Sanchez-Cano, C.; Moat, J.; Dowson, C. G.; Williams, E. G. L.; Locock, K. E. S.; Hartlieb, M.; Perrier, S. Sequence Control as a Powerful Tool for Improving the Selectivity of Antimicrobial Polymers. *ACS Appl. Mater. Interfaces* **2017**, *9* (46), 40117−40126.
(41) Zhou, C.; Qi, X.; Li, P.; Chen, W. N.; Mouad, L.; Chang, M. W.; Leong, S. S. J.; Chan-Park, M. B. High Potency and Broad-Spectrum Antimicrobial Peptides Synthesized *via* Ring-Opening Polymerization of α-Aminoacid-N-Carboxyanhydrides. *Biomacromolecules* **2010**, *11* (1), 60−67.
(42) Im, H.; Dwidar, M.; Mitchell, R. J. *Bdellovibrio bacteriovorus* HD100, a Predator of Gram-Negative Bacteria, Benefits Energetically from *Staphylococcus aureus* Biofilms without Predation. *ISME J.* **2018**, *12* (8), 2090−2095.
(43) Liu, D.; Choi, S.; Chen, B.; Doerksen, R. J.; Clements, D. J.; Winkler, J. D.; Klein, M. L.; DeGrado, W. F. Nontoxic Membrane-Active Antimicrobial Arylamide Oligomers. *Angew. Chem., Int. Ed.* **2004**, *43* (9), 1158−1162.
(44) De Jong, D. H.; Singh, G.; Bennett, W. F. D.; Arnarez, C.; Wassenaar, T. A.; Schäfer, L. V.; Periole, X.; Tieleman, D. P.; Marrink, S. J. Improved Parameters for the Martini Coarse-Grained Protein Force Field. *J. Chem. Theory Comput.* **2013**, *9* (1), 687−697.
(45) Flinner, N.; Schleiff, E. Dynamics of the Glycophorin a Dimer in Membranes of Native-Like Composition Uncovered by Coarse-Grained Molecular Dynamics Simulations. *PLoS One* **2015**, *10* (7), 1−16.
(46) Qi, Y.; Ingólfsson, H. I.; Cheng, X.; Lee, J.; Marrink, S. J.; Im, W. CHARMM-GUI Martini Maker for Coarse-Grained Simulations with the Martini Force Field. *J. Chem. Theory Comput.* **2015**, *11* (9), 4486−4494.
(47) Abraham, M. J.; Murtola, T.; Schulz, R.; Páll, S.; Smith, J. C.; Hess, B.; Lindah, E. Gromacs: High Performance Molecular Simulations through Multi-Level Parallelism from Laptops to Supercomputers. *SoftwareX* **2015**, *1−2*, 19−25.
(48) Marrink, S. J.; Risselada, H. J.; Yefimov, S.; Tieleman, D. P.; De Vries, A. H. The MARTINI Force Field: Coarse Grained Model for Biomolecular Simulations. *J. Phys. Chem. B* **2007**, *111* (27), 7812−7824.
(49) Bussi, G.; Donadio, D.; Parrinello, M. Canonical Sampling through Velocity Rescaling. *J. Chem. Phys.* **2007**, *126* (1), 014101.
(50) Berendsen, H. J. C.; Postma, J. P. M.; Van Gunsteren, W. F.; Dinola, A.; Haak, J. R. Molecular Dynamics with Coupling to an External Bath. *J. Chem. Phys.* **1984**, *81* (8), 3684−3690.
(51) Parrinello, M.; Rahman, A. Polymorphic Transitions in Single Crystals: A New Molecular Dynamics Method. *J. Appl. Phys.* **1981**, *52* (12), 7182−7190.
(52) Hess, B.; Bekker, H.; Berendsen, H. J. C.; Fraaije, J. G. E. M. LINCS: A Linear Constraint Solver for Molecular Simulations. *J. Comput. Chem.* **1997**, *18* (12), 1463−1472.

https://doi.org/10.1021/acsnano.1c02644
ACS Nano 2021, 15, 9143−9153